
Input margins can predict generalization too

Anonymous Author(s)

Affiliation

Address

email

Abstract

1 Understanding generalization in deep neural networks is an active area of research.
2 A promising avenue of exploration has been that of margin measurements: the
3 shortest distance to the decision boundary for a given sample or its representation
4 internal to the network. While margins have been shown to be correlated with
5 the generalization ability of a model when measured at its hidden representations
6 (hidden margins), no such link between large margins and generalization has been
7 established for *input margins*. We show that while input margins are not gener-
8 ally predictive of generalization, they can be if the search space is appropriately
9 constrained. We develop such a measure based on input margins, which we refer
10 to as ‘constrained margins’. The predictive power of this new measure is demon-
11 strated on the ‘Predicting Generalization in Deep Learning’ (PGDL) dataset and
12 contrasted with hidden representation margins. We find that constrained margins
13 achieve highly competitive scores and outperform other margin measurements in
14 general.

15 1 Introduction

16 Our understanding of the generalization ability of deep neural networks (DNNs) remains incomplete.
17 Various bounds on the generalization error for classical machine learning models have been proposed
18 based on the complexity of the hypothesis space [1, 2]. However, this approach paints an unfinished
19 picture when considering modern DNNs [3]. Generalization in DNNs is an active field of study and
20 updated bounds are proposed on an ongoing basis [4, 5, 6, 7].

21 A complementary approach to developing theoretical bounds is to develop empirical techniques that
22 are able to predict the generalization ability of certain families of DNN models. The ‘Predicting
23 Generalization in Deep Learning’ (PGDL) challenge, exemplifies such an approach. The challenge
24 was held at NeurIPS 2020 [8] and provides a useful test bed for evaluating *complexity measures*,
25 where a complexity measure is a scalar-valued function that relates a model’s training data and
26 parameters to its expected performance on unseen data. Such a predictive complexity measure would
27 not only be practically useful but could lead to new insights into how DNNs generalize.

28 In this work, we focus on classification margins in deep neural classifiers. It is important to note that
29 the term ‘margin’ is, often confusingly, used to refer to 1) output margins [9], 2) input margins [10],
30 and 3) hidden margins [11], interchangeably. Here (1) is a measure of the difference in class output
31 values, while (2) or (3) is concerned with measuring the distance from a sample to its nearest decision
32 boundary in either input or hidden representation space, respectively. In this work, we focus on input
33 and hidden margins.

34 While margins measured at the hidden representations of deep neural classifiers have been shown to
35 be predictive of a model’s generalization, this link has not been established for input space margins.
36 We show that, in several circumstances, the classical definition of input margin does *not* predict
37 generalization, but a direction-constrained version of this metric does: a quantity we refer to as

38 *constrained margins*. By measuring margins in directions of ‘high utility’, that is, directions that are
39 expected to be more useful to the classification task, we are able to better capture the generalization
40 ability of a trained DNN.

41 We make several contributions:

- 42 1. Demonstrate the first link between large input margins and generalisation performance, by
43 developing a new input margin-based complexity measure that achieves highly competitive
44 performance on the PGDL benchmark and outperforms several contemporary complexity
45 measures.
- 46 2. Show that margins do not necessarily need to be measured at multiple hidden layers to be
47 predictive of generalization, as suggested in [11].
- 48 3. Provide a new perspective on margin analysis and how it applies to DNNs, that of finding
49 high utility directions along which to measure the distance to the boundary instead of
50 focusing on finding the shortest distance.

51 **2 Background**

52 This section provides an overview of existing work on 1) measuring classification margins and their
53 relationship to generalization, and 2) the PGDL challenge and related complexity measures.

54 **2.1 Classification Margins and Generalization**

55 Considerable prior work exists on understanding classification margins in machine learning mod-
56 els [12, 13]. The relation between margin and generalization is well understood for classifiers such as
57 support vector machines (SVMs) under statistical learning theory [1]. However, the non-linearity and
58 high dimensionality of DNN decision boundaries complicate such analyses, and precisely measuring
59 these margins is considered intractable [14, 15].

60 A popular technique (which we revisit in this work) is to approximate the classification margin using
61 a first-order Taylor approximation. Elsayed et al. [16] use this method in both the input and hidden
62 space, and then formulate a loss function that maximizes these margins. However, while this results
63 in a measurable increase in margin, it does not result in any significant gains in test accuracy. In a
64 seminal paper, Jiang et al. [11] utilize the same approximation in order to predict the generalization
65 gap of a set of trained networks by training a linear regression model on a summary of their hidden
66 margin distributions. Natekar and Sharma [17] demonstrate that this measure can be further improved
67 if margins are measured using the representations of Mixup [18] or augmented training samples.
68 Similarly, Chuang et al. [6] introduce novel generalization bounds and slightly improve on this metric
69 by proposing an alternative cluster-aware normalization scheme (k -variance [19]).

70 Input margins are generally considered from the point of view of adversarial robustness, and many
71 techniques have been developed to generate adversarial samples on or near the decision boundary.
72 Examples include: the Carlini and Wagner Attack [20], Projected Gradient Descent [21], and
73 DeepFool [22]. Some of these studies have investigated the link between adversarial robustness
74 and generalization, often concluding that an inherent trade-off exists [23, 24, 25]. However, this
75 conclusion and its intricacies are still being debated [26].

76 Yousefzadeh and O’Leary [14] formulate finding a point on the decision boundary as a constrained
77 minimization problem, which is solved using an off-the-shelf optimization method. While this method
78 is more precise, it comes at a great computational cost. To alleviate this, dimensionality reduction
79 techniques are used in the case of image data to reduce the number of input features. In this case, the
80 classification margin is used for the purpose of model interpretability.

81 In this work we propose a modification to the Taylor approximation of the input classification margin
82 (and its iterative alternative DeepFool) in order for it to be more predictive of generalization.

83 **2.2 Predicting Generalization in Deep Learning**

84 The objective of this challenge was to design a complexity measure to rank models according to their
85 generalization gap. More precisely, participants only had access to a set of trained models, along with

86 their parameters and training data, and were tasked with ranking the models within each set according
87 to their generalization gap. Each solution was then evaluated on how well its ranking aligns with the
88 true ranking on a held-out set of tasks, which was unknown to the competitors.

89 In total, there are 550 trained models across 8 different tasks and 6 different image classification
90 datasets, where each task refers to a set of models trained on the same dataset with varying hyperpa-
91 rameters and subsequent test accuracy. Tasks 1, 2, 4, and 5 were available for prototyping and tuning
92 complexity measures, while Task 6 to 9 were used as a held-out set. There is no task 3. The final
93 average score on the test set was the only metric used to rank the competitors. Conditional mutual
94 information (CMI) is used as evaluation metric, which measures the conditional mutual information
95 between the complexity measure and true generalization gap, given that a set of hyperparameter
96 types are observed. This is done in order to prevent spurious correlations resulting from specific
97 hyperparameters, a step towards establishing whether a causal relationship exists.

98 All models were trained to approximately the same, near zero, training loss. Note that this implies that
99 ranking models according to either their generalization gap or test accuracy is essentially equivalent.

100 Several interesting solutions were developed during the challenge: In addition to the modification of
101 hidden margins mentioned earlier, the winning team [17] developed several prediction methods based
102 on the internal representations of each model. Their best-performing method measures clustering
103 characteristics of hidden layers (using Davies-Bouldin Index [27]), and combines this with the
104 model’s accuracy on Mixup-augmented training samples. In a similar fashion, the runners-up based
105 their metrics on measuring the robustness of trained networks to augmentations of their training
106 data [28].

107 After the competition’s completion, the dataset was made publicly available, inspiring further research:
108 Schiff et al. [29] generated perturbation response curves that ‘capture the accuracy change of a given
109 network as a function of varying levels of training sample perturbation’ and develop statistical
110 measures from these curves. They produced eleven complexity measures with different types of
111 sample Mixup and statistical metrics.

112 While several of the methods rely on using synthetic samples (e.g. Mixup), Zhang et al. [30] take
113 this to the extreme and generate an artificial test set using pretrained generative adversarial networks
114 (GANs). They demonstrate that simply measuring the classification accuracy on this synthetic test set
115 is very predictive of a model’s generalization. While practically useful, this method does not make a
116 link between any characteristics of the model and its generalization ability.

117 **3 Theoretical approach**

118 This section provides a theoretical overview of the proposed complexity measure. We first explain our
119 intuition surrounding classification margins, before mathematically formulating constrained margins.

120 **3.1 Intuition**

121 A correctly classified training sample with a large margin can have more varied feature values,
122 potentially due to noise, and still be correctly classified. However, as we will show, input margins
123 are not generally predictive of generalization. This observation is supported by literature regarding
124 adversarial robustness, where it has been shown that adversarial retraining (which increases input
125 margins) can negatively affect generalization [23, 25].

126 Stutz et al. [26] provide a plausible reason for this counter-intuitive observation: Through the use
127 of Variational Autoencoder GANs they show that the majority of adversarial samples leave the
128 class-specific data manifold of the samples’ class. They offer the intuitive example of black border
129 pixels in the case of MNIST images, which are zero for all training samples. Samples found on
130 the decision boundary which manipulate these border pixels have a zero probability under the data
131 distribution, and they do not lie on the underlying manifold.

132 We leverage this intuition and argue that any input margin measure that relates to generalization
133 should measure distances along directions that do not rely on spurious features in the input space.
134 The intuition is that, while nearby decision boundaries exist for virtually any given training sample,
135 these nearby decision boundaries are likely in directions which are not inherently useful for test set
136 classification, i.e. they diverge from the underlying data manifold.

137 More specifically, we argue that margins should be measured in directions of ‘high utility’, that is,
 138 directions that are expected to be useful for characterising a given dataset, while ignoring those of
 139 lower utility. In our case, we approximate these directions by defining high utility directions as
 140 directions which explain a large amount of variance in the data. We extract these using Principal
 141 Component Analysis (PCA). While typically used as a dimensionality reduction technique, PCA can
 142 be interpreted as learning a low-dimensional manifold [31], albeit a linear one. In this way, the PCA
 143 manifold identifies subspaces that are thought to contain the variables that are truly relevant to the
 144 underlying data distribution, which the out-of-sample data is assumed to also be generated from. In
 145 the following section, we formalize such a measure.

146 3.2 Constrained Margins

147 We first formulate the classical definition of an input margin [14], before adapting it for our purpose.
 148 Let $f : X \rightarrow \mathbb{R}^{|N|}$ denote a classification model with a set of output classes $N = \{1 \dots n\}$, and
 149 $f_k(\mathbf{x})$ the output value of the model for input sample \mathbf{x} and output class k . For a correctly classified
 150 input sample \mathbf{x} , the goal is to find the closest point $\hat{\mathbf{x}}$ on the decision boundary between the true
 151 class i (where $i = \arg \max_k (f_k(\mathbf{x}))$) and another class $j \neq i$. Formally, $\hat{\mathbf{x}}$ is found by solving the
 152 constrained minimization problem:

$$\arg \min_{\hat{\mathbf{x}} \in [L, U]} \|\mathbf{x} - \hat{\mathbf{x}}\|_2 \quad (1)$$

153 with L and U the lower and upper bounds of the search space, respectively, such that

$$f_i(\hat{\mathbf{x}}) = f_j(\hat{\mathbf{x}}) \quad (2)$$

154 for i and j as above.

155 The margin is then given by the Euclidean distance between the input sample, \mathbf{x} , and its corresponding
 156 sample on the decision boundary, $\hat{\mathbf{x}}$. We now adapt this definition in order to define a ‘constrained
 157 margin’. Let the set $P = \{\mathbf{p}_1, \mathbf{p}_2, \dots, \mathbf{p}_m\}$ denote the first m principal component vectors of the
 158 training dataset, that is, the m orthogonal principal components which explain the most variance.
 159 Such principal components are straightforward to extract by first standardizing (z normalizing) each
 160 feature individually, and then calculating the eigenvectors of the covariance matrix of the standardized
 161 training data.

162 We now restrict $\hat{\mathbf{x}}$ to any point consisting of the original sample \mathbf{x} plus a linear combination of these
 163 principal component vectors, that is, for some coefficient vector $\mathbf{B} = [\beta_1, \beta_2, \dots, \beta_m]$

$$\hat{\mathbf{x}} \triangleq \mathbf{x} + \sum_{i=1}^m \beta_i \mathbf{p}_i \quad (3)$$

164 Substituting $\hat{\mathbf{x}}$ into the original objective function of Equation (1), the new objective becomes

$$\min_{\beta} \left\| \sum_{i=1}^m \beta_i \mathbf{p}_i \right\|_2 \quad (4)$$

165 such that Equation (2) is approximated within a certain tolerance. For this definition of margin, the
 166 search space is constrained to a lower-dimensional subspace spanned by the principal components
 167 with point \mathbf{x} as origin, and the optimization problem then simplifies to finding a point on the decision
 168 boundary within this subspace. By doing so, we ensure that boundary samples that rely on spurious
 169 features (that is, in directions of low utility) are not considered viable solutions to Equation (1). Note
 170 that this formulation does not take any class labels into account for identifying high utility directions.

171 While it is possible to solve the constrained minimization problem using a constrained optimizer [14],
 172 we approximate the solution by adapting the previously mentioned first-order Taylor approximation
 173 [16, 32], which greatly reduces the computational cost. The Taylor approximation of the
 174 constrained margin $d(\mathbf{x})$ for a sample \mathbf{x} between classes i and j when using an $L2$ norm is given by

$$d(\mathbf{x}) = \frac{f_i(\mathbf{x}) - f_j(\mathbf{x})}{\| [\nabla_{\mathbf{x}} f_i(\mathbf{x}) - \nabla_{\mathbf{x}} f_j(\mathbf{x})] \mathbf{P}^T \|_2} \quad (5)$$

175 where \mathbf{P} is the $m \times n$ matrix formed by the top m principal components with n input features. The
 176 derivation of Equation (5) is included in the supplementary material.

177 The value $d(\mathbf{x})$ only approximates the margin and the associated discrepancy in Equation (2) can be
 178 large. In order to reduce this to within a reasonable tolerance, we apply Equation (5) in an iterative
 179 manner, using a modification of the well-known DeepFool algorithm [22]. DeepFool was defined
 180 in the context of generating adversarial samples with the smallest possible perturbation, which is in
 181 effect very similar to finding the nearest point on the decision boundary with the smallest violation of
 182 Equation (2).

183 To extract the DeepFool constrained margin for some sample \mathbf{x} , the Taylor approximation of the
 184 constrained margin is calculated between the true class i and all other classes j , individually. A small
 185 step (scaled by a set learning rate) is then taken in the lower-dimensional subspace in the direction
 186 corresponding to the class with smallest margin. This point is then transformed back to the original
 187 feature space and the process is repeated until the distance changes less than a given tolerance in
 188 comparison to the previous iteration. The exact process to calculate a DeepFool constrained margin is
 189 described in Algorithm 1. Note that we also clip $\hat{\mathbf{x}}$ according to the minimum and maximum feature
 190 values of the dataset after each step, which ensures that the point stays within the bound constraints
 191 expressed in Equation 1. While this is likely superfluous when generating normal adversarial samples
 192 – they are generally very close to the original \mathbf{x} – it is a consideration when the search space is
 193 constrained, with clipped margins performing better. (See the supplementary material for an ablation
 194 analysis of clipping.)

Algorithm 1 DeepFool constrained margin calculation

Input: Sample \mathbf{x} , classifier f , principal components \mathbf{P}

Parameter: Stopping tolerance δ , Learning rate γ , Maximum iterations max

Output: Distance d_{best} , Equality violation v_{best}

```

1:  $\hat{\mathbf{x}} \leftarrow \mathbf{x}, i \leftarrow \arg \max_k f_k(\mathbf{x}), d \leftarrow 0, v_{best} \leftarrow \infty, c \leftarrow 0$ 
2: while  $c \leq max$  do
3:   for  $j \neq i$  do
4:      $o_j \leftarrow f_i(\hat{\mathbf{x}}) - f_j(\hat{\mathbf{x}})$ 
5:      $\mathbf{w}_j \leftarrow [\nabla f_i(\hat{\mathbf{x}}) - \nabla f_j(\hat{\mathbf{x}})]\mathbf{P}^T$ 
6:   end for
7:    $l \leftarrow \arg \min_{j \neq i} \frac{|o_j|}{\|\mathbf{w}_j\|_2}$ 
8:    $\mathbf{r} \leftarrow \frac{|o_l|}{\|\mathbf{w}_l\|_2} \mathbf{w}_l \mathbf{P}$ 
9:    $\hat{\mathbf{x}} \leftarrow \hat{\mathbf{x}} + \gamma \mathbf{r}$ 
10:   $\hat{\mathbf{x}} \leftarrow \text{clip}(\hat{\mathbf{x}})$ 
11:   $v \leftarrow |o_l|$ 
12:   $d \leftarrow \|\mathbf{x} - \hat{\mathbf{x}}\|_2$ 
13:  if  $v \geq v_{best}$  or  $|d - d_{best}| < \delta$  then
14:    return  $d_{best}, v_{best}$ 
15:  else
16:     $v_{best} \leftarrow v$ 
17:     $d_{best} \leftarrow d$ 
18:     $c \leftarrow c + 1$ 
19:  end if
20: end while
21: return  $d_{best}, v_{best}$ 

```

195 **4 Results**

196 We investigate the extent to which constrained margins are predictive of generalization by comparing
 197 the new method with current alternatives. In Section 4.1 we describe our experimental setup.
 198 Following this, we do a careful comparison between our metric and existing techniques based on
 199 standard input and hidden margins (Section 4.2) and, finally, we compare with other complexity
 200 measures (Section 4.3).

201 **4.1 Experimental setup**

202 For all margin-based measures our indicator of generalization (complexity measure) is the mean
203 margin over 5 000 randomly selected training samples, or alternatively the maximum number available
204 for tasks with less than 5 000 training samples. Only correctly classified samples are considered, and
205 the same training samples are used for all models of the same task. To compare constrained margins
206 to input and hidden margins we rank the model test accuracies according to the resulting indicator
207 and calculate the Kendall’s rank correlation [33], as used in [34]. This allows for a more interpretable
208 comparison than CMI. (As CMI is used throughout the PGDL challenge, we also include the resulting
209 CMI scores in the supplementary material.) To compare constrained margins to published results of
210 other complexity measures, we measure CMI between the complexity measure and generalization
211 gap and contrast this with the reported scores of other methods.

212 As a baseline we calculate the **standard input margins** (‘Input’) using the first order Taylor approxi-
213 mation (Equation 5 without the subspace transformation), as we find that it achieves better results
214 than the iterative DeepFool variant and is therefore the stronger baseline; see the supplementary
215 material for a full comparison.

216 Creating a complexity measure from **hidden margins** (‘Hidden’) raises the question of which hidden
217 layers to consider. Jiang et al. [11] consider three equally spaced layers, Natekar and Sharma [17]
218 consider all layers, and Chuang et al. [6] consider either the first or last layer only. We calculate
219 the mean hidden margin (using the Taylor approximation) for all these variations and find that for
220 the tasks studied here, using the first layer performs best, while the mean over all layers comes in
221 second. We include both results here. (A full analysis is included in the supplementary material.) We
222 normalize each layer’s margin distribution by following [11], and divide each margin by the total
223 feature variance at that layer.

224 Our **constrained margin** complexity measure (‘Constrained’) is obtained using Algorithm 1, although
225 in practice we implement this in a batched manner. Empirically, we find that the technique is not
226 very sensitive with regard to the selection of hyperparameters and a single learning rate ($\gamma = 0.25$),
227 tolerance ($\delta = 0.01$), and max iterations ($max = 100$) is used across all experiments. The number of
228 principal components for each dataset is selected by plotting the explained variance (of the train data)
229 per principal component in decreasing order on a logarithmic scale and applying the elbow method
230 using the Kneedle algorithm from Satopaa et al [35]. This results in a very low-dimensional search
231 space, ranging from 3 to 8 principal components for the seven unique datasets considered.

232 In order to prevent biasing our metric to the PGDL test set (tasks 6 to 9) we did not perform any tuning
233 or development of the complexity measure using these tasks, nor do we tune any hyperparameters
234 per task. The choice of principal component selection algorithm was done after a careful analysis of
235 Tasks 1 to 5 only, see additional details in the supplementary material. In terms of computational
236 expense, we find that calculating the entire constrained margin distribution only takes 1 to 2 minutes
237 per model on an Nvidia A30.

238 **4.2 Margin complexity measures**

239 In Table 1 we show the Kendall’s rank correlation obtained when ranking models according to
240 constrained margin, standard input margins, and hidden margins. It can be observed that standard
241 input margins are not predictive of generalization for most tasks and, in fact, show a negative
242 correlation for some. This unstable behaviour is supported by ongoing work surrounding adversarial
243 robustness and generalization [23, 24, 25]. Furthermore, we observe a very large performance gap
244 between constrained and standard input margins, and an increase from 0.24 to 0.66 average rank
245 correlation is observed by constraining the margin search. This strongly supports our initial intuitions.

246 In the case of hidden margins, performance is more competitive, however, constrained margins
247 still outperform hidden margins on 6 out of 8 tasks. One also observes that the selection of hidden
248 layers can have a very large effect, and the discrepancy between the two hidden-layer selections is
249 significant. Given that our constrained margin measurement is limited to the input space, there are
250 several advantages: 1) no normalization is required, as all models share the same input space, and 2)
251 the method is more robust when comparing models with varying topology, as no specific layers need
252 to be selected.

Table 1: Kendall’s rank correlation between mean margin and test accuracy for constrained, standard input, and hidden margins using the first or all layer(s). Models in Task 4 are trained with batch normalization while models in Task 5 are trained without. There is no Task 3.

Task	Architecture	Dataset	Constrained	Input	Hidden (1st)	Hidden (all)
1	VGG	CIFAR10	0.8040	0.0265	0.5794	0.7825
2	NiN	SVHN	0.8672	0.6841	0.7037	0.8281
4	FCN	CINIC10	0.6651	0.6251	0.7958	0.2707
5	FCN	CINIC10	0.2292	0.3571	0.5427	0.1329
6	NiN	OxFlowers	0.8008	-0.1351	0.4427	0.2839
7	NiN	OxPets	0.5027	0.3215	0.3623	0.3481
8	VGG	FMNIST	0.6004	-0.1233	-0.0656	0.1859
9	NiN	CIFAR10 (augmented)	0.8145	0.1573	0.7097	0.4556
Average			0.6605	0.2392	0.5088	0.4110

253 4.3 Other complexity measures

254 To further assess the predictive power of constrained margins, we compare our method to the reported
 255 CMI scores of several other complexity measures. We compare against three solutions from the
 256 winning team [17], as well as the best solutions from two more recent works [6, 29], where that of
 257 Schiff et al. [29] has the highest average test set performance we are aware of. We do not compare
 258 against pretrained GANs [30]. The original naming of each method is kept. Of particular relevance
 259 are the *MM* and *AM* columns, which are hidden margins applied to Mixup and Augmented samples,
 260 as well as *kV*-Margin and *kV*-GN-Margin which are output and hidden margins with *k*-Variance
 261 normalization, respectively. The results of this comparison are shown in Table 2.

262 One observes that constrained margins achieve highly competitive scores, and in fact, outperform all
 263 other measures on 4 out of 8 tasks. It is also important to note that the *MM* and *AM* columns show
 264 that hidden margins can be improved in some cases if they are measured using the representations of
 265 Mixup or augmented training samples. That said, these methods still underperform on average in
 266 comparison to constrained input margins, which do not rely on any form of data augmentation.

Table 2: Conditional Mutual Information (CMI) scores for several complexity measures on the PGDL dataset. Acronyms: *DBI*=Davies Bouldin Index, *LWM*=Label-wise Mixup, *MM*=Mixup Margins, *AM*=Augmented Margins, *kV*=*k*-Variance, *GN*=Gradient Normalized, *Gi*=Gini coefficient, *Mi*=Mixup. Test set average is the average over tasks 6 to 9. There is no Task 3. †Indicates a margin-based measure.

Task	Natekar and Sharma			Chuang et al.		Schiff et al.	Ours
	DBI*LWM	MM†	AM†	<i>kV</i> - Margin 1st†	<i>kV</i> -GN- Margin 1st†	PCA Gi&Mi	Constrained Margin†
1	00.00	01.11	05.73	05.34	17.95	0.04	39.37
2	32.05	47.33	44.60	26.78	44.57	38.08	51.12
4	31.79	43.22	47.22	37.00	30.61	33.76	21.48
5	15.92	34.57	22.82	16.93	16.02	20.33	05.12
6	43.99	11.46	08.67	06.26	04.48	40.06	30.52
7	12.59	21.98	11.97	02.07	03.92	13.19	12.60
8	09.24	01.48	01.28	01.82	00.61	10.30	13.54
9	25.86	20.78	15.25	15.75	21.20	33.16	51.46
Test set average	22.92	13.93	09.29	06.48	07.55	23.62	27.03

267 5 A closer look

268 In this section we do a further analysis of constrained margins. In Section 5.1 we investigate how the
 269 performance of constrained margins changes when lower utility subspaces are considered, whereafter
 270 we discuss limitations of the method in Section 5.2.

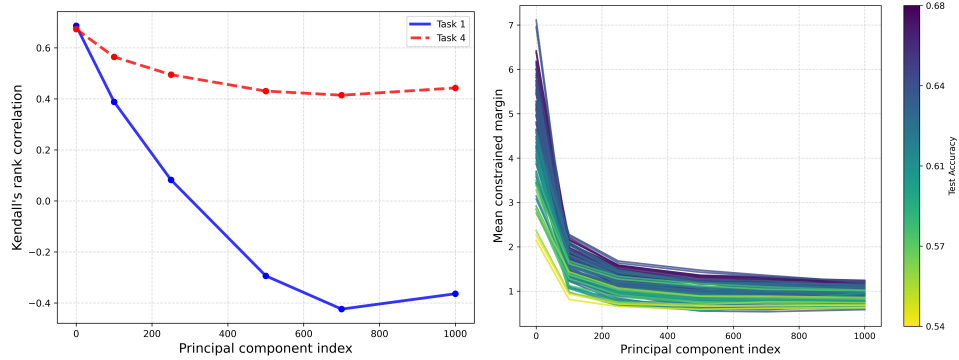


Figure 1: Comparison of high to low utility directions using subspaces spanned by 10 principal components, x-axis indicates the first component in each set of principal components. Left: Kendall’s rank correlation for Task 1 (blue solid line) and 4 (red dashed line). Right: Mean constrained margin for models from Task 4.

271 5.1 High to low utility

272 We examine how high utility directions compare to those of lower utility when calculating constrained
 273 margins. This allows us to further test our approach, as one would expect that margins measured
 274 using the lower-ranked principal components should be less predictive of a model’s performance.

275 We calculate the mean constrained margin using select subsets of 10 contiguous principal components
 276 in descending order of explained variance. For example, we calculate the constrained margins using
 277 components 1 to 10, then 100 to 109, etc. This allows us to calculate the distance to the decision
 278 boundary using 10 dimensional subspaces of decreasing utility. We, once again, make use of 5 000
 279 training samples. We restrict ourselves to analysing the training set of tasks (tasks 1-5) and consider
 280 one task where constrained margins perform very well (Task 1) and one with poorer performance
 281 (Task 4). Figure 1 (left) shows the resulting Kendall’s rank correlation for each subset of principal
 282 components indexed by the first component in each set (principal component index). The right-hand
 283 side shows the mean margin of all models from Task 4 at each subset.

284 As expected, the first principal components lead to margins that are more predictive of generalization.
 285 We see a gradual decrease in predictive power when considering later principal components. Task
 286 1 especially suffers this phenomenon, reaching negative correlations. This supports the idea that
 287 utilizing the directions of highest utility is a necessary aspect of input margin measurements. Addi-
 288 tionally, one observes that the mean margin also rapidly decreases after the first few sets of principal
 289 components. After the point shown here (index 1 000), we find that the mean margin increases as
 290 DeepFool struggles to find samples on the decision boundary within the bound constraints. Due
 291 to this, it is difficult to draw any conclusions from an investigation of the lower-ranked principal
 292 components. This also points to the notion that the adversarial vulnerability of modern DNNs is in
 293 part due to nearby decision boundaries in the directions of the mid-tier principal components (the
 294 range of 100 to 1 000).

295 5.2 Limitations

296 It has been demonstrated that our proposed metric performs well and aligns with our initial intuition.
 297 However, there are also certain limitations that require explanation. Empirically we observe that, for
 298 tasks where constrained margins perform well, they do so across all hyperparameter variations, with
 299 the exception of depth. This is illustrated in Figure 2 (left), which shows the mean constrained margin
 300 versus test accuracy for Task 1. We observe that sets of networks with two and six convolutional
 301 layers, respectively, each exhibit a separate relationship between margin and test accuracy. This
 302 discrepancy is not always as strongly present: for Task 6 all three depth configurations show a more
 303 similar relationship, as observed on the right of Figure 2, although the discrepancy is still present. The
 304 same trend holds for all tasks where it is observed (1, 2, 4, 6, 9). It appears that shallower networks
 305 model the input space in a distinctly different fashion than their deeper counterparts.

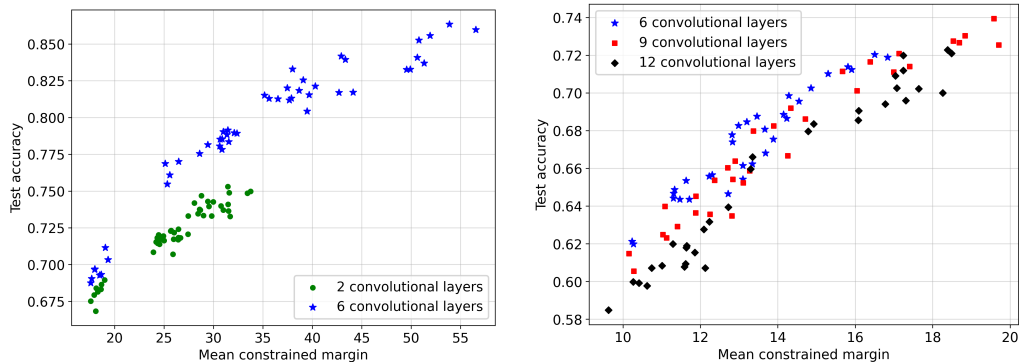


Figure 2: Mean constrained margin versus test accuracy for PGDL Task 1 (left) and 6 (right). Left: Models with 2 (green circle) and 6 (blue star) convolutional layers. Right: Models with 6 (blue star), 9 (red square), and 12 (black diamond) convolutional layers.

306 For tasks such as 5 and 7, where constrained margins perform more poorly, there is no single
 307 hyperparameter that appears to be the culprit. We do note that the resulting scatter plots of margin
 308 versus test accuracy never show points in the lower right (large margin but low generalization) or
 309 upper left (small margin but high generalization) quadrants. It is therefore possible that a larger
 310 constrained margin is always beneficial to a model’s generalization, even though it is not always
 311 fully descriptive of its performance. Finally, while our approach to selecting the number of principal
 312 components is experimentally sound, the results can be further improved if the optimal number is
 313 known, see the supplementary material for details.

314 6 Conclusion

315 We have shown that constraining input margins to high utility subspaces can significantly improve
 316 their predictive power i.t.o generalization. Specifically, we have used the principal components of the
 317 data as a proxy for identifying these subspaces, which can be considered a rough approximation of
 318 the underlying data manifold.

319 Constraining the search to a warped subspace and using Euclidean distance to measure closeness is
 320 equivalent to defining a new distance metric on the original space. We are therefore, in effect, seeking
 321 a relevant distance metric to measure the closeness of the decision boundary. Understanding the
 322 requirements for such a metric remains an open question. Unfortunately, current approximations and
 323 methods for finding points on the decision boundary are largely confined to L_p metrics. The positive
 324 results achieved with the current PCA-and-Euclidean-based approach provide strong motivation that
 325 this is a useful avenue to pursue. Furthermore, we believe that constrained margins can be used
 326 as a tool to further probe generalization, similar to the large amount of work that has been done
 327 surrounding standard input margins and characterization of decision boundaries.

328 In conclusion, we propose constraining input margins to make them more predictive of generalization
 329 in DNNs. It has been demonstrated that this greatly increases the predictive power of input margins,
 330 and also outperforms hidden margins and several other contemporary methods on the PGDL tasks.
 331 This method has the benefits of requiring no per-layer normalization, no arbitrary selection of hidden
 332 layers, and does not rely on any form of surrogate test set (e.g. data augmentation or synthetic
 333 samples).

334 **References**

- 335 [1] Vladimir N Vapnik. An overview of statistical learning theory. *IEEE Transactions on Neural*
336 *Networks*, 10(5):988–999, 1999.
- 337 [2] Vladimir Koltchinskii and Dmitry Panchenko. Empirical margin distributions and bounding the
338 generalization error of combined classifiers. *The Annals of Statistics*, 30(1):1–50, 2002.
- 339 [3] Chiyuan Zhang, Samy Bengio, Moritz Hardt, Benjamin Recht, and Oriol Vinyals. Understanding
340 deep learning (still) requires rethinking generalization. *Communications of the ACM*, 64(3):107–
341 115, 2021.
- 342 [4] Sanjeev Arora, Rong Ge, Behnam Neyshabur, and Yi Zhang. Stronger generalization bounds
343 for deep nets via a compression approach. In *International Conference on Machine Learning*
344 *(ICML)*, pages 254–263. PMLR, 2018.
- 345 [5] Kenji Kawaguchi, Leslie Pack Kaelbling, and Yoshua Bengio. *Generalization in Deep Learning*.
346 *Mathematical Aspects of Deep Learning*. Cambridge University Press, 2022.
- 347 [6] Ching-Yao Chuang, Youssef Mroueh, Kristjan Greenewald, Antonio Torralba, and Stefanie
348 Jegelka. Measuring generalization with optimal transport. *Advances in Neural Information*
349 *Processing Systems*, 34:8294–8306, 2021.
- 350 [7] Sanae Lotfi, Marc Anton Finzi, Sanyam Kapoor, Andres Potapczynski, Micah Goldblum,
351 and Andrew Gordon Wilson. PAC-Bayes compression bounds so tight that they can explain
352 generalization. In *Advances in Neural Information Processing Systems*, 2022.
- 353 [8] Yiding Jiang, Pierre Foret, Scott Yak, Daniel M Roy, Hossein Mobahi, Gintare Karolina
354 Dziugaite, Samy Bengio, Suriya Gunasekar, Isabelle Guyon, and Behnam Neyshabur. Neurips
355 2020 competition: Predicting generalization in deep learning. *arXiv preprint arXiv:2012.07976*,
356 2020.
- 357 [9] Peter L Bartlett, Dylan J Foster, and Matus J Telgarsky. Spectrally-normalized margin bounds
358 for neural networks. *Advances in Neural Information Processing Systems*, 30, 2017.
- 359 [10] Jure Sokolić, Raja Giryes, Guillermo Sapiro, and Miguel RD Rodrigues. Robust large margin
360 deep neural networks. *IEEE Transactions on Signal Processing*, 65(16):4265–4280, 2017.
- 361 [11] Yiding Jiang, Dilip Krishnan, Hossein Mobahi, and Samy Bengio. Predicting the generalization
362 gap in deep networks with margin distributions. In *International Conference on Learning*
363 *Representations*, 2018.
- 364 [12] Bernhard E Boser, Isabelle M Guyon, and Vladimir N Vapnik. A training algorithm for optimal
365 margin classifiers. In *Proceedings of the fifth annual workshop on Computational Learning*
366 *Theory*, pages 144–152, 1992.
- 367 [13] Kilian Q. Weinberger and Lawrence K. Saul. Distance metric learning for large margin nearest
368 neighbor classification. *Journal of Machine Learning Research*, 10(9):207–244, 2009.
- 369 [14] Roozbeh Yousefzadeh and Dianne P. O’Leary. Deep learning interpretation: Flip points
370 and homotopy methods. In Jianfeng Lu and Rachel Ward, editors, *Proceedings of The First*
371 *Mathematical and Scientific Machine Learning Conference*, volume 107 of *Proceedings of*
372 *Machine Learning Research*, pages 1–26. PMLR, 20–24 Jul 2020.
- 373 [15] Yaoqing Yang, Rajiv Khanna, Yaodong Yu, Amir Gholami, Kurt Keutzer, Joseph E Gonzalez,
374 Kannan Ramchandran, and Michael W Mahoney. Boundary thickness and robustness in learning
375 models. *Advances in Neural Information Processing Systems*, 33:6223–6234, 2020.
- 376 [16] Gamaleldin Elsayed, Dilip Krishnan, Hossein Mobahi, Kevin Regan, and Samy Bengio. Large
377 margin deep networks for classification. *Advances in Neural Information Processing Systems*,
378 31, 2018.
- 379 [17] Parth Natekar and Manik Sharma. Representation based complexity measures for predicting
380 generalization in deep learning. *arXiv preprint arXiv:2012.02775*, 2020.

- 381 [18] Hongyi Zhang, Moustapha Cisse, Yann N. Dauphin, and David Lopez-Paz. mixup: Beyond
382 empirical risk minimization. In *International Conference on Learning Representations*, 2018.
- 383 [19] Justin Solomon, Kristjan Greenewald, and Haikady Nagaraja. k-variance: A clustered notion of
384 variance. *SIAM Journal on Mathematics of Data Science*, 4(3):957–978, 2022.
- 385 [20] Nicholas Carlini and David Wagner. Towards evaluating the robustness of neural networks. In
386 *IEEE Symposium on Security and Privacy*, pages 39–57. IEEE, 2017.
- 387 [21] Aleksander Madry, Aleksandar Makelov, Ludwig Schmidt, Dimitris Tsipras, and Adrian Vladu.
388 Towards deep learning models resistant to adversarial attacks. In *International Conference on*
389 *Learning Representations*, 2018.
- 390 [22] Seyed-Mohsen Moosavi-Dezfooli, Alhussein Fawzi, and Pascal Frossard. DeepFool: a simple
391 and accurate method to fool deep neural networks. In *Proceedings of the IEEE Conference on*
392 *Computer Vision and Pattern Recognition*, pages 2574–2582, 2016.
- 393 [23] Dimitris Tsipras, Shibani Santurkar, Logan Engstrom, Alexander Turner, and Aleksander
394 Madry. Robustness May Be at Odds with Accuracy. In *International Conference on Learning*
395 *Representations*, 2019.
- 396 [24] Dong Su, Huan Zhang, Hongge Chen, Jinfeng Yi, Pin-Yu Chen, and Yupeng Gao. Is Robustness
397 the Cost of Accuracy?—A Comprehensive Study on the Robustness of 18 Deep Image Classifi-
398 cation Models. In *Proceedings of the European Conference on Computer Vision (ECCV)*, pages
399 631–648, 2018.
- 400 [25] Aditi Raghunathan, Sang Michael Xie, Fanny Yang, John Duchi, and Percy Liang. Adversarial
401 Training Can Hurt Generalization. In *ICML Workshop on Identifying and Understanding Deep*
402 *Learning Phenomena*, 2019.
- 403 [26] David Stutz, Matthias Hein, and Bernt Schiele. Disentangling Adversarial Robustness and
404 Generalization. In *Proceedings of the IEEE/CVF Conference on Computer Vision and Pattern*
405 *Recognition*, pages 6976–6987, 2019.
- 406 [27] David L Davies and Donald W Bouldin. A cluster separation measure. *IEEE Transactions on*
407 *Pattern Analysis and Machine Intelligence*, (2):224–227, 1979.
- 408 [28] Dhruva Kashyap, Natarajan Subramanyam, et al. Robustness to augmentations as a generaliza-
409 tion metric. *arXiv preprint arXiv:2101.06459*, 2021.
- 410 [29] Yair Schiff, Brian Quanz, Payel Das, and Pin-Yu Chen. Predicting Deep Neural Network
411 Generalization with Perturbation Response Curves. *Advances in Neural Information Processing*
412 *Systems*, 34:21176–21188, 2021.
- 413 [30] Yi Zhang, Arushi Gupta, Nikunj Saunshi, and Sanjeev Arora. On Predicting Generalization
414 using GANs. In *International Conference on Learning Representations*, 2022.
- 415 [31] Geoffrey E Hinton, Peter Dayan, and Michael Revow. Modeling the Manifolds of Images of
416 Handwritten Digits. *IEEE Transactions on Neural Networks*, 8(1):65–74, 1997.
- 417 [32] Ruitong Huang, Bing Xu, Dale Schuurmans, and Csaba Szepesvári. Learning with a Strong
418 Adversary. *arXiv preprint arXiv:1511.03034*, 2015.
- 419 [33] M. G. Kendall. A New Measure of Rank Correlation. *Biometrika*, 30(1-2):81–93, 06 1938.
- 420 [34] Yiding Jiang, Behnam Neyshabur, Hossein Mobahi, Dilip Krishnan, and Samy Bengio. Fantastic
421 generalization measures and where to find them. In *International Conference on Learning*
422 *Representations*, 2019.
- 423 [35] Ville Satopaa, Jeannie Albrecht, David Irwin, and Barath Raghavan. Finding a "kneede" in a
424 haystack: Detecting knee points in system behavior. In *2011 31st international Conference on*
425 *Distributed Computing systems workshops*, pages 166–171. IEEE, 2011.